

## TIME-DEPENDENT BEHAVIOR OF CRACKED CONCRETE BEAMS UNDER SUSTAINED LOADING

R. SARKHOSH<sup>\*\*†</sup>, J.C. WALRAVEN<sup>†</sup> AND J.A. DEN UIJL<sup>†</sup>

<sup>†</sup> Delft University of Technology  
Faculty of Civil Engineering and Geosciences  
2628 CN, Delft, the Netherlands  
e-mail: r.sarkhosh@tudelft.nl, www.tudelft.nl

**Key words:** Time-dependent fracture, Concrete beam, Crack

**Abstract:** Under sustained loading, the propagation of cracks in concrete is assumed to be related to the elastic deformation, material parameters and time. Based on the fictitious crack model (FCM), a finite element method is proposed to explain the behavior of cracks in time using current constitutive relations to approximate the time-dependent crack strain. Experiments have been performed on small concrete specimens to determine the cracking strain and to validate the finite element model. For flexural cracks, a creep coefficient model is adopted for bulk creep and a cracking strain rate based on test results is employed. For shear cracks fracture mode II is considered as well. The development of concrete strength in time is taken into account. The model is applied to predict the behavior of a cracked concrete beam subjected to sustained loading. Finally a comparison is made between the results of different approaches.

### 1 INTRODUCTION

Developing numerical models to simulate the time-dependent behavior of quasi-brittle materials such as concrete and masonry has always been a major issue in civil engineering [1-6]. Traditionally, numerical simulations are based on finite element methods based on discrete crack approach or the smeared crack model. This paper aims at modelling the time-dependent behavior of concrete by means of the discrete crack approach.

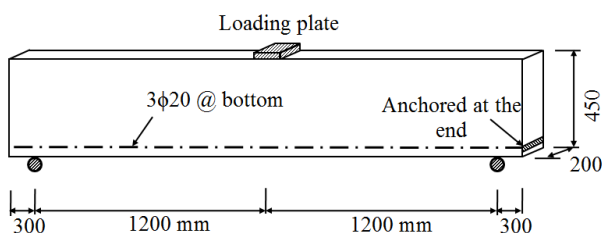


**Figure 1:** Sustained loading tests on concrete beams [7].

Long-term tests on large-scale concrete beams [7] without shear reinforcement (Figure 1), which had been tested for more than two years under sustained loading close to the ultimate shear capacity (load ratio ranging from 87% to 95%) under climate controlled condition, showed that sustained loading has no significant effect on the shear capacity. Although many flexural and shear cracks occurred, the beams carried the load for a long time. The tests showed that crack formation took place only some days after loading, but after a week the cracks stabilized and became dormant. After these tests, it was decided to evaluate the behavior of single-cracked concrete beams under sustained loading by means of experiments and numerical modeling. This part of the research is presented in this paper.

## 2 FICTITIOUS CRACK MODEL

Fracture in quasi-brittle materials such as concrete and masonry is different from that of real brittle materials. Tension cracking at a notch or a pre-existing crack is associated with a localized narrow band of damaged material ahead of the crack tip referred to as the fracture process zone (FPZ) and the stresses within this zone exhibit significant softening [8].

The FPZ in front of a notch or a crack normally develops in a tensile stress field and consequently the properties of this zone are similar to those of the fracture zone in a direct tensile test. The stress transferring capability of FPZ depends on the width of the slit in the stressed direction.

The stress transferring crack is not a real crack but can be considered as a fictitious crack and therefore the model described above is called the Fictitious Crack Model. When using the Fictitious Crack Model the following assumptions are made:

- In the traditional fictitious crack model, the static tensile strength serves as a criterion for initiation of the crack.
- The fracture zone develops in the direction perpendicular to the first principal stress.
- The material in the fracture zone is partly damaged but it is still able to transfer stress. The stress transferring capability depends on the local deformation of the fracture zone in the direction of the first principal stress. In the calculations the fracture zone is normally replaced by a stress transferring crack and the stress transferring capability depends on the width of the crack in the stressed direction according to the softening curve.
- The width of the fracture zone is obtained according to the strain in the direction of first principal stress.
- Outside the fracture zone the material behavior is assumed to be elastic.

By using the Fictitious Crack Model, it is possible to study the development of the fracture zone, the initiation of crack growth and the propagation of the crack through the material [9].

## 3 CREEP

Time dependent behavior of quasi-brittle materials is usually described by means of creep or relaxation. In a uniaxial creep test, the stress history  $\sigma(t)$  is prescribed by:

$$\sigma(t) = \begin{cases} 0 & t < 0 \\ \sigma_0 & t \geq 0 \end{cases} \quad (1)$$

where  $\sigma_0$  is a constant stress applied at time  $t=0$ .

The creep strain  $\varepsilon(t)$  is expressed as:

$$\varepsilon(t) = J(t) \sigma_0 \quad (2)$$

where  $J(t)$  is the creep compliance.

For creep simulation, creep may be divided into two main processes regarding the period of consideration; short-term bulk creep and long-term bulk creep. For a duration of less than several months, short-term bulk creep can be calculated from Bažant's Model B3 [10]:

$$\phi(t, t') = E(t') J(t, t') - I$$

$$J(t, t') = q_1 + C_0(t, t') + C_d(t, t', t_0) \quad (3)$$

Where  $E(t')$  is the modulus of elasticity at loading age  $t'$ ,  $q_1$  is the instantaneous strain due to unit stress,  $C_0(t, t')$  is a compliance function for basic creep and  $C_d(t, t', t_0)$  is an additional compliance function due to simultaneous drying. A simplified compliance function based on a double power law was proposed earlier by Bažant and Chern [11]:

$$J(t, t') = 1/E_0 [1 + \phi(t'^{1/3} + 0.05)(t - t')^{1/8}] \quad (4)$$

where  $E_0$  is 1.5~2.0E. In this study model B3 has been used for modeling together with the EC2 recommendation for creep [12].

For long-term periods exceeding several months, the creep coefficient  $\phi(t)$  which is the ratio of the creep displacement to the elastic displacement at time  $t$  is expressed by an exponential growth function:

$$\phi(t) = \phi_\infty (1 - e^{-t/T}) \quad (5)$$

where  $\phi_\infty$  is the creep coefficient at time infinity and  $T$  is the retardation time at which 63% of the maximum value of  $\phi$  is obtained.

## 4 CRACK RATE DEPENDENCY

The process of the breakage of bond in the

FPZ, which causes the softening law for the crack opening to be rate-dependent, can be modeled by a cohesive crack growth model in a viscoelastic material [13]. However, based on the experimental results, the opening of the crack in time shows rather viscoplastic behaviour, see section 5, therefore in this paper it is tried to develop an elastic-viscoplastic model with damage for the rate dependency of the crack strain. Typically the viscoplastic constitutive equations are developed from a number of spring and dashpot elements arranged in series and parallel.

Two commonly used models are the generalized Maxwell chain and the generalized Burger's model where in the former the same strain is shared across all the elements and the stress is additive, and in the generalized Burger's model the strains are additive and the stress is the same for each element. The generalized Burger's model will be adopted here because it shares the same framework as classical visco-plasticity models and allows for non-linearity based on stress to be accommodated more easily [14]. It can be seen from Figure 2 that the generalized Burger's model comprises an elastic element in series with a number of viscoelastic (Kelvin-Voigt) elements and a viscoplastic element. The stresses transmitted through each element and the strains are additive such that:

$$\varepsilon(t) = \varepsilon_{el}(t) + \varepsilon_{ve}(t) + \varepsilon_{vp}(t) \quad (6)$$

where  $\varepsilon$ ,  $\varepsilon_{el}$ ,  $\varepsilon_{ve}$ ,  $\varepsilon_{vp}$  are the total elastic, viscoelastic and viscoplastic strain components at time  $t$ . The elastic component can be drawn as:

$$\varepsilon_{el}(t) = \sigma(t) / E_0 \quad (7)$$

where  $\sigma$  is stress and  $E_0$  is modulus of elasticity of the elastic element. The viscoelastic and viscoplastic components can be calculated using the Hereditary Integral formulation [15]:

$$\varepsilon_{ve}(t) = J_{ve}(0)\sigma(t) + \int_0^t \frac{dJ_{ve}(t-t')}{d(t-t')} \sigma(t') dt' \quad (8)$$

$$\varepsilon_{vp}(t) = J_{vp}(0)\sigma(t) + \int_0^t \frac{dJ_{vp}(t-t')}{d(t-t')} \sigma(t') dt' \quad (9)$$

Where  $J_{ve}$  and  $J_{vp}$  are the viscoelastic and viscoplastic creep compliances and  $t'$  is a dummy integration variable, which is in our case the age of the specimen when the first load is applied. It can be shown that the first derivatives of the viscoelastic and viscoplastic creep compliances and the initial creep compliances for the generalized Burger's model shown in Figure 2 are given by:

$$\frac{dJ_{ve}(t-t')}{d(t-t')} = \sum_{i=1}^N \frac{1}{\eta_i} e^{-(t-t')/\tau_i} \quad (10)$$

$$\tau_i = \eta_i / E_i \quad (11)$$

$$\frac{dJ_{vp}(t-t')}{d(t-t')} = \frac{1}{\eta_0} \quad (12)$$

Where  $\eta_i$  and  $E_i$  are viscosity and modulus of elasticity of the  $i^{th}$  Voigt viscoelastic element,  $\eta_0$  is the viscosity of the viscoplastic element with the boundary condition of  $J_{ve}(0) = J_{vp}(0) = 0$ . This constitutive model needs to be expressed in incremental forms of elastic strain  $\Delta\varepsilon_{el}$ , viscoelastic strain  $\Delta\varepsilon_{ve}$  and viscoplastic strain  $\Delta\varepsilon_{vp}$ , which can be written after simplification as:

$$\Delta\varepsilon_{el} = {}^{t+\Delta t}\varepsilon_{el} - {}^t\varepsilon_{el} = \Delta\sigma / E_0 \quad (13)$$

$$\Delta\varepsilon_{ve} \cong \sum_{i=1}^N \left[ {}^t\varepsilon_{ve}^i \left( e^{-\frac{\Delta t}{\tau_i}} - 1 \right) + \frac{\Delta t}{\eta_i} e^{-\frac{\Delta t}{2\tau_i}} \left( {}^t\sigma + \frac{\Delta\sigma}{2} \right) \right] \quad (14)$$

$$\Delta\varepsilon_{vp} \cong \frac{\Delta t}{\eta_0} \left( {}^t\sigma + \frac{\Delta\sigma}{2} \right) \quad (15)$$

where,  ${}^{t+\Delta t}\varepsilon_{el}$  and  ${}^t\varepsilon_{el}$  are the elastic strains at

time  $t$  and  $t+\Delta t$  respectively,  ${}^t\sigma$  is the stress at time  $t$ ,  $\Delta\sigma$  is the stress increment,  $N$  is the number of Voigt elements,  ${}^t\varepsilon_{ve}^i$  is the viscoelastic strain for the  $i^{th}$  Voigt element at time  $t$ .

The above mentioned rheological model with three Voigt elements is used to evaluate the cracking strain rate according to the test results and is employed in the following model.

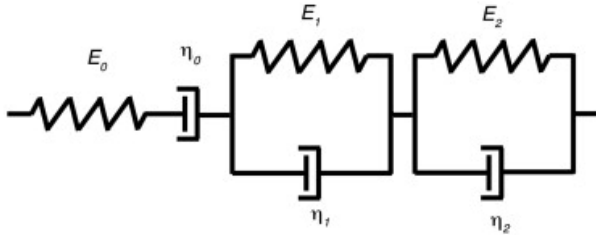


Figure 2: Generalized Burger's model.

## 5 EXPERIMENTAL PROGRAM

The experimental investigation relates to the behavior of plain concrete beams with a single notch under sustained loading, see Figure 3. The notch is located in the bottom side of the beam at midspan. The experimental program comprised a total number of 15 specimens with the same concrete mix design, eight of which were subjected to short-term loading.

On one hand, the test results refer to measured material characteristics such as development of concrete compressive strength and on the other hand, the measured crack width and length are given for each specimen. The crack mouth opening (with a measuring length of 40 mm) and midspan deflection were measured at both front and rear of the beam by means of LVDT's connected to the computer.

### 5.1 Short-term results

The results of the eight short-term tests are given in Figure 4. The average ultimate capacity of specimens that failed in short-term loading (including two beams that were supposed to be loaded in long-term but failed before the desired load was applied), was 2.74 kN with a coefficient of variation of 12.9%.

The end of elastic zone in P-CMOD curves

is observed at a concrete strain ranging from 0.000112 to 0.000180 with an average value of 0.000146.

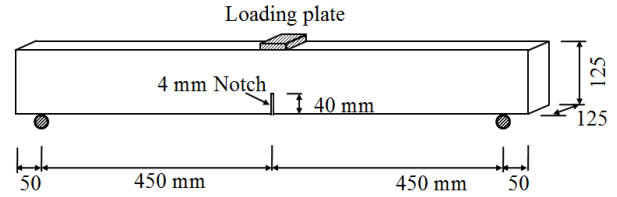


Figure 3: Geometry of the specimens.

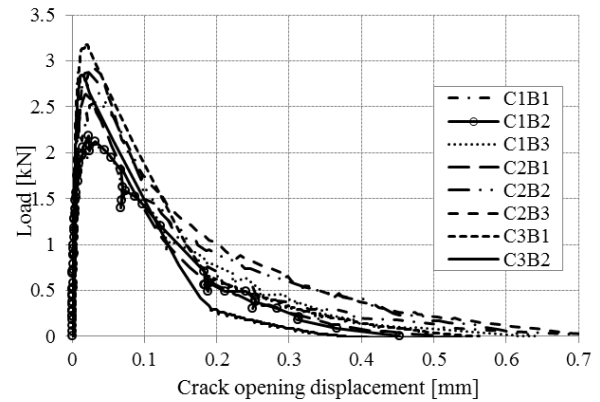


Figure 4: Short-term loading, P-CMOD curves.

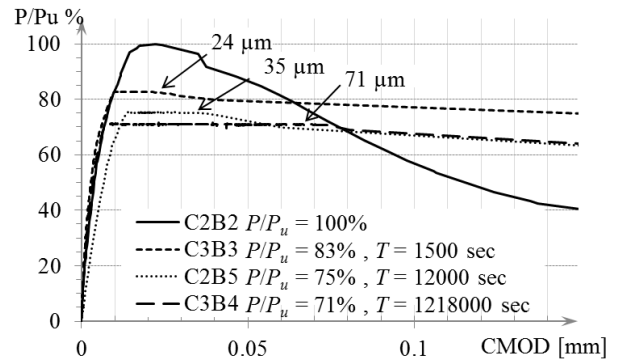


Figure 5: Long-term loading, P-CMOD curves.

### 5.2 Long-term results

In order to get insight into the effect of load under sustained loading, the applied load is given as a ratio to the ultimate short-term capacity. The load ratios in the following graphs are based on the average value of all short-term tests.

In Figure 5, the load ratio is represented along the vertical axis, whereas along the horizontal axis the displacements are shown. Together with the long-term tests, one of the

short-term tests is presented for a better comparison. As shown in this figure the lower is the load ratio, the larger is the CMOD at failure. E.g. specimens C3B3, C2B5 and C3B4, which were loaded at 83%, 75% and 71% of ultimate capacity, had a maximum CMOD of 0.024, 0.035 and 0.071 mm, respectively, at the time of failure.

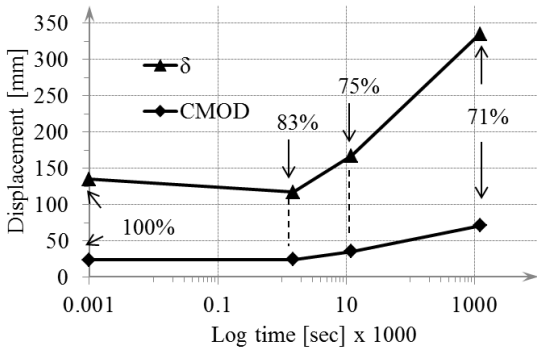


Figure 6: Maximum displacement versus time to failure

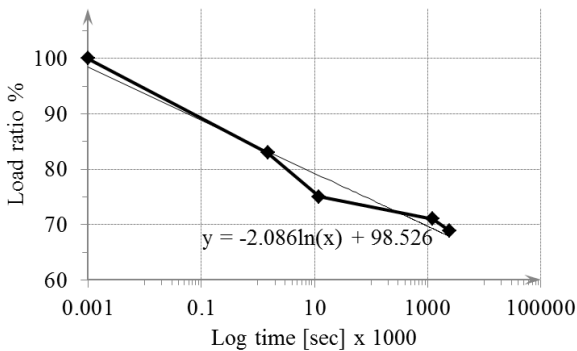


Figure 7: Time to failure versus load ratio.

In Figure 6, the magnitudes of CMOD and  $\delta$  for different load ratios are presented in a graph versus time. These curves confirm that the longer the time to failure, the larger the displacement at failure. In the other words under sustained loading, the concrete fails due to larger strains depending on the load ratio/time of loading.

Moreover, the load ratio versus the corresponding time to the failure of the beam under sustained loading is shown in Figure 7. These graphs show a logarithmic relationship between the sustained-loading time and the load ratio.

### 5.3 Cracking strain rate

The cracking strain rate is found from the relation between the crack opening strain measured from the moment that the sustained loading is fully applied and the time. As shown in Figure 8, three different stages can be distinguished in this graph; the Primary Stage, which can be fitted with an elastic and a viscoelastic model, according to section 4, the Secondary Stage, which can be fitted with a viscoplastic model and the Tertiary Stage that is the fracture stage. The latter is not fitted with any model since that is the irreversible stage where fracturing already occurred. As mentioned before, this Burger's model with three Voigt elements will be used in the following FE modeling.

In Figure 9, the relative crack opening displacements of three tests loaded at 71%, 75% and 83% of the ultimate capacity are shown in a semi-logarithmic graph as a function of time.  $CMOD_u$  is the crack mouth opening displacement of short-term tests when the load is at peak.

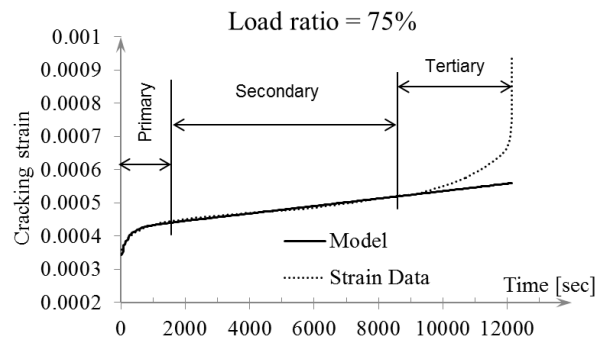


Figure 8: Three stages of cracking strain development under sustained loading

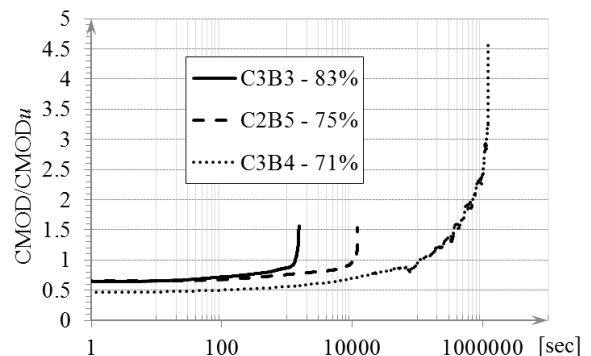


Figure 9: CMOD and time to failure for different load ratios.

## 6 LINEAR ELASTIC FRACTURE MODEL (LEFM)

Linear elastic fracture models have been widely used to predict the crack path development for quasi-brittle materials such as concrete, even for complex trajectories [16]. With step-wise linear increment, the initiation and the propagation of the crack can be simulated to a global response [5], which can be reproduced by changing the material properties in every step.

Based on the fictitious crack model [17, 18] and using the finite element method, a LEFM is employed to predict the time dependent behavior of a flexural crack.

Under long-term loading, the strain due to the creep effect in the high stress zone around the fictitious crack tip may reach the critical strain, so that crack formation can occur below the static tensile strength. Therefore the criterion should be adjusted to account for the time effect.

Time dependent problems are often solved by dividing time into small increments. Under sustained loading, it is usual to evaluate incremental creep strains from stresses at the beginning of the time step. In order to obtain the strain as a function of time, a bulk creep function should be used; either an existing recommended function for creep (e.g. the Eurocode 2 recommendation for creep [12] or Model B3 [10]) or an experiment-based function by means of a rheological model can be used. The Poisson ratio can be assumed to be time independent (being equal to 0.2) [19]. The structure is considered to be macroscopically homogeneous in the sense that the same  $J(t, t')$  applies to every point of the homogenizing continuum throughout the bulk of the structure.

The finite element method with discrete approach has been chosen in modeling of FPZ. A special program was developed in MATLAB and used in all calculations. For the simplification in modeling of a flexural crack, the crack propagation path is assumed to be known in advance and is chosen to coincide with the boundary conditions while in the shear crack, the unknown crack path

propagates between the elements with corresponding regeneration of finite element mesh.

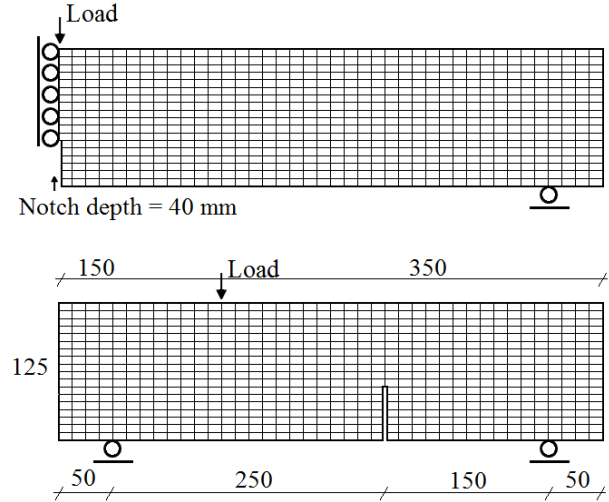


**Figure 10:** Top: FE model of the specimen in Figure 3. Only half of the beam is modeled due to symmetry. Bottom: FE model of the beam with notch in shear.

Material is modeled as linear elastic by using 4-node plane stress elements. Every single element has four individual nodes which are connected to the nodes of the next element through a connection matrix. The connection of two/three/four neighbor nodes is lost when the crack passes through the elements. To solve the problem, an iterative method is required to update the stiffness matrix and find the nodal forces in the fictitious crack. Moreover, the stress redistribution due to crack opening in time is considered. The nonlinear behavior is modeled by an interactive linear model that approximates the crack propagation into step-wise linear increments and regenerates the meshes in each segment.

The step by step linear elastic model was derived on basis of the following considerations:

- A. By assembling of stiffness matrix, the nodal stress vector can be found as:  $\{\sigma\} = [D] \{\varepsilon\}$  where  $[D]$  is the constitutive matrix and  $\{\varepsilon\} = [B] \{u^e\}$ ,  $[B]$  is the strain displacement matrix and  $\{u^e\}$  is element displacement vector.
- B. The crack propagation is assumed to occur in the interface between the elements in

linear increments. Under sustained loading, the incremental creep strains from the principal stresses at the beginning of the time segment can be evaluated. The crack path follows the maximum principal stress in the adjacent nodes. The criterion for which the crack will begin to propagate is the total strain (including the elastic and creep strains) at the crack tip exceeding the critical strain  $\varepsilon_{cr}$ . At this point, the corresponding node pair opens (2<sup>nd</sup> segment) and the mesh regenerates. Yet the crack width in fracture zone is small enough to carry the tensile forces, the fracture zone is modeled by ‘nodal forces’ which act as resisting stress along the crack face. The resisting stresses acting across the fracture zone are replaced by nodal forces in the finite element model.

- C. For each increment, an iterative method is used to evaluate the nodal forces in the FPZ, according to the following method; With the new stiffness matrix based on new mesh generation, the nodal displacements and thus the crack width in the first iteration  $w_{i,iter=1}$ , is found. The intensity of these forces at each step depends on the width of the fictitious crack according to the  $\sigma$ - $w$  curve of the material. In the linear elastic model, the width of the fictitious crack depends on the size of the applied load  $P$ , and when the nodal forces (corresponding to the width of crack) apply to the nodes, the crack width reduces. With the obtained nodal force at the end of iteration, vector  $\{F\}_{nodes}$  is assembled with the nodal forces. The total applied force on the model is:  $\{F\}_{iter=2} = \{F\}_P + \{F\}_{nodes}$ . With the new force vector  $\{F\}_{iter=2}$ , in the second iteration, the nodal displacements and the crack width are evaluated. Subsequently, a new vector of the nodal forces should be adjusted to the new crack width. It is obvious that  $w_{i,iter=2} < w_{i,iter=1}$  due to the resistant forces applied on the node. The iteration continues until the difference of crack widths in two following iterations converges to zero. This would be the end of segment 2.

- D. At the end of each increment the criterion for the propagation of the crack should be considered. The crack in static modeling propagates until the criterion  $\varepsilon \geq \varepsilon_{cr}$  is met.
- E. After the static modeling and evaluating the stresses in front of the notch tip, the creep strain can be assessed in different time intervals, by means of compliance functions, see Figure 11. Meeting the criterion  $\varepsilon \geq \varepsilon_{cr}$ , the corresponding node pairs are opened and step C should be followed.

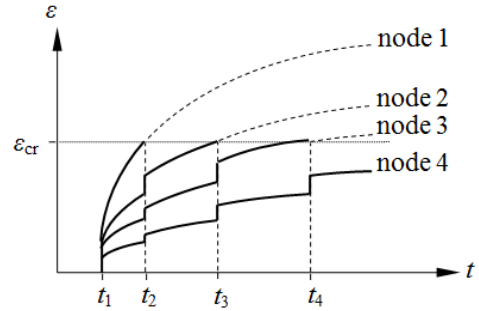


**Figure 11:** Strain development of strain at nodes in front of crack tip in time.

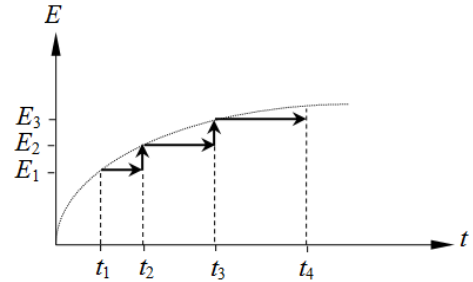


**Figure 12:** Modulus of elasticity used at each load step.  $t_1, t_2$  represent the time at the beginning of segments 1, 2

- F. In this way, the crack propagation in the given time interval can be evaluated. Under high load ratios, the creep develops faster and the failure (opening of all node pairs in front of crack tip) occurs at early age, while for low loading ratios, failure may never occur.

## 7 TIME DEPENDENT PARAMETERS

The following time-dependent parameters are taken into consideration into this model:

## 7.1 Bulk creep

Short-term bulk creep for loading times up to 4 months and long-term bulk creep for longer times are considered in this model. The results of Model B3 [10] are compared to the Eurocode2 creep recommendations [12].

## 7.2 Crack rate dependency

As mentioned in section 6, the creep strain can be evaluated in a stabilized stress distribution at each time interval. However, this assumption needs modification when the rate dependency of the fracture process is considered. This means that due to the time dependent crack width, the stress intensity and the nodal force vector  $\{F\}_{\text{nodes}}$  in FPZ changes. Accordingly, the stress should be redistributed in the model in each time interval. Based on the cracking strain rate which is evaluated from the test results, sections 4 and 5, the model is modified.

## 7.3 Concrete strength

The compressive strength of concrete at an age  $t$  depends on the type of cement, temperature and curing conditions. For a mean temperature of 20°C and curing in accordance with EN 12390 the compressive strength of concrete at various ages  $f_{cm}(t)$  may be estimated from the following expressions [20]:

$$f_{cm}(t) = \beta_{cc}(t) f_{cm} \quad (16)$$

$$\beta_{cc}(t) = \exp\{s [1 - (28/t)^{0.5}]\} \quad (17)$$

where  $f_{cm}$  is the mean compressive strength at 28 days,  $t$  is the age of concrete in days and  $s$  is a coefficient which depends on the strength class of cement.

The development of tensile strength with time also is strongly influenced by curing and drying conditions as well as by the dimensions of the structural members. As a first approximation it may be assumed that the tensile strength  $f_{ctm}(t)$  is equal to:

$$f_{ctm}(t) = [\beta_{cc}(t)] \alpha f_{ctm} [20] \quad (18)$$

where,  $\alpha = 1$  for  $t < 28$  days and  $\alpha = 2/3$  for  $t \geq 28$  days

## 7.4 Modulus of elasticity

The variation of  $E$  modulus with time can be estimated by the following expressions:

$$E_{cm}(t) = (\beta_{cc})^{0.3} E_{cm} [12] \quad (19)$$

$$E_{cm}(t) = [\beta_{cc}(t)]^{0.5} E_{cm} [20] \quad (20)$$

The modulus of elasticity, as it is developing in time, should be recalculated when the crack develops in time but remains constant until the next node pair opens. The new modulus ( $E_1, E_2, \dots$ ) in each time interval ( $t_2-t_1, t_3-t_2, \dots$ ) should be taken into account according to Figure 12. It is not allowed to consider the developing modulus of elasticity within the time interval, as it is impossible to have a negative strain in linear tension.

## 7.5 Fracture energy mode I, ${}^I G_F$

The fracture energy of concrete, defined as the energy required for propagating a tensile crack of unit area, should be determined by related tests. In absence of experimental data,  ${}^I G_F$  [N/m] for ordinary normal weight concrete may be estimated from one of the following expressions.

$${}^I G_F = 73 \cdot f_{cm}^{0.18} [12] \quad (21)$$

$${}^I G_F = a_d \cdot f_{cm}^{0.7} [21] \quad (22)$$

where,  $a_d$  is a coefficient that depends on the maximum aggregate size and is equal to 4, 6 or 10 for maximum aggregate size of 8, 16 and 32 mm, respectively.

As the concrete strength develops in time, the fracture energy requires to be modified in each time interval, according to the method used to evaluate the modulus of elasticity in time.

As mentioned before, the fracture zone, in front of the notch-tip is modeled by ‘nodal forces’ and the intensity of these forces of course depends on the width of the fictitious crack according to the  $\sigma$ - $w$  curve of the material. Following [17, 22] a bilinear softening traction-separation curve is used in this paper as shown in Figure 13, with the following values:

$$f_{tm} = f_{ctmo} \ln(1 + f_{cm} / f_{cmo}) \quad (23)$$

$$w' = 2^I G_F / f_t - 0.15 w_c \quad (24)$$

$$w_c = \alpha_F^I G_F / f_{tm} \quad (25)$$

where,  $f_{ctmo} = 2.12$  MPa and  $f_{cmo} = 10$  MPa [20].  $f_{tm}$  is mean tensile strength.  $w'$  is the crack opening at the neck [mm],  $w_c$  is the crack opening [mm] for  $\sigma_{ct} = 0$  and  $\alpha_F$  depends on the maximum size of aggregates  $d_{max}$  that is equal to 8, 7, and 5 corresponding to  $d_{max} = 8, 16, 32$  mm, respectively.

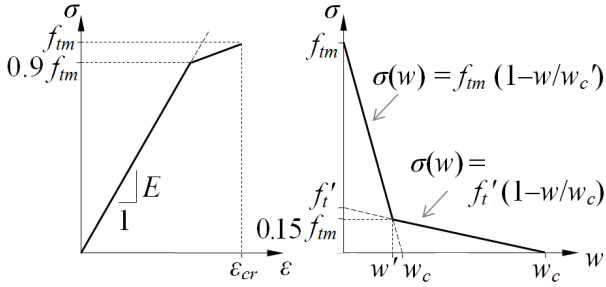


**Figure 13:** Bilinear  $\sigma$ - $\epsilon$  and bilinear softening traction-separation curve ( $\sigma$ - $w$  curve).

## 7.6 Fracture energy mode II, ${}^II G_F$

It was shown by Gálvez et al [16] that for quasi-brittle materials under global mixed mode loading the crack grows with a predominantly local mode I fracture. It has also been stated that Mode II fracture energy may only have a slight effect on the growth of the shear crack. However, for different geometries of the mixed mode fracture, the results may be different.

For mixed mode fracture, the interaction between normal stress,  $\sigma$ , and tangential stress,  $\tau$ , should be taken into account. Since the creep strains are evaluated based on the principal stress, it is not required to check the strain in different directions. The tension-resistant forces (tensile strength) perpendicular to the crack face are taken into account based on the tension softening curve (fracture energy mode I). Potentially, the slip-resistant forces in FPZ parallel to the crack can be evaluated according to the cohesion strength (fracture energy mode II).

To get insight into the influence of the cohesion  $c$ , to the results of shear capacity of the concrete, two models are proposed. In the

first model the initiation and growth of the shear crack is reported by pure Mode I while in the second model, the mixed mode (I and II) is considered which means that the slip-resistant forces due to cohesion softening curve are taken into account, see Figure 14.

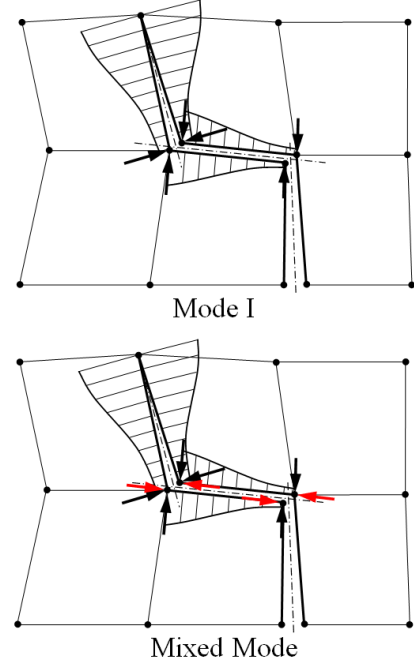


**Figure 14:** Path of shear crack. The red vectors represent the cohesion in the middle part.

Using a quadrilateral mesh and allowing the shear crack path to find its way between the elements, the aggregate interlock can be simulated when the fracture mode II is considered. It seems more realistic than using triangular meshes with a smooth shear crack as the shear crack faces are naturally rough. With a very fine mesh, the possible inconsistencies due to the mesh type will be avoided.

## 8 RESULTS OF MODELLING

The results of FE modeling are presented in the following divisions:

### 8.1 Time-dependent behavior and total fracture

With the proposed FE method, the propagation of the critical crack can be estimated in time until fracture of the beam. In Figure 15, the propagation of the crack is shown by means of the total creep in the nodes

in front of the notch tip. As soon as the total creep exceeds the critical creep, which is here 0.00015, the corresponding node opens and the model is regenerated. It is shown that under 60% of the ultimate capacity, the failure occurs at 72 days after opening of the 5<sup>th</sup> node (crack length = 28 mm).

In Figure 16, the estimated time for the fracture of concrete beam is presented in different load ratios together with the experimental results. The material properties given as input to the program are based on the tests performed on the concrete specimens.

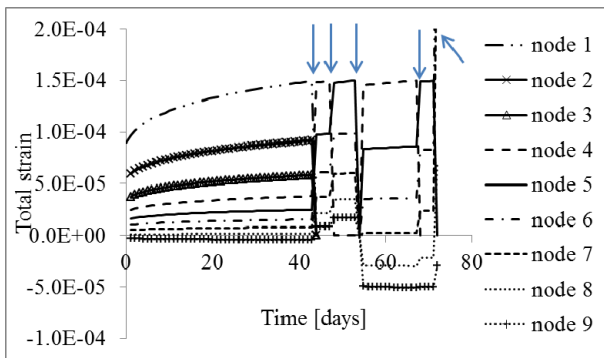


Figure 15: Opening of the nodes in front of notch tip in time (Load ratio = 60%).

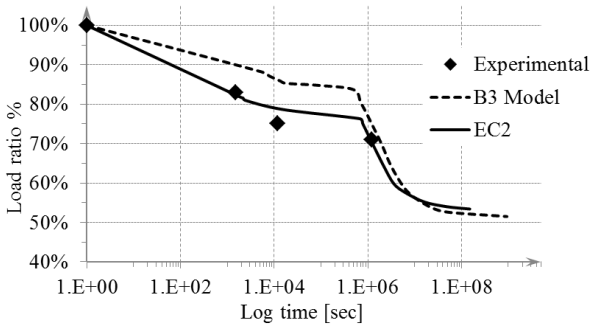


Figure 16: Estimated time for fracture of beam according to B3 model & EC2 creep coefficient.

### 8.2 Effect of compliance function

The estimated fracture time in this model depends on the compliance function that is used. Considering that the tensile strength in American codes (e.g. ACI) is higher than in the European code (EC2), the compliance function of Model B3 [10] gives a slower rate of crack propagation in comparison with the EC2 creep coefficient, see Figure 16.

### 8.3 Effect of cracking strain rate

As shown in section 5.3, the cracking strain rate with an elastic-visco-plastic model is considered in this model. Figure 17 presents a comparison of two models with and without cracking rate dependency, confirming that if the cracking rate dependency is not considered in the model, the fracture process would be longer than expected, especially in case of high load ratio where the crack is already formed. The effect of cracking strain rate is well presented in [6].

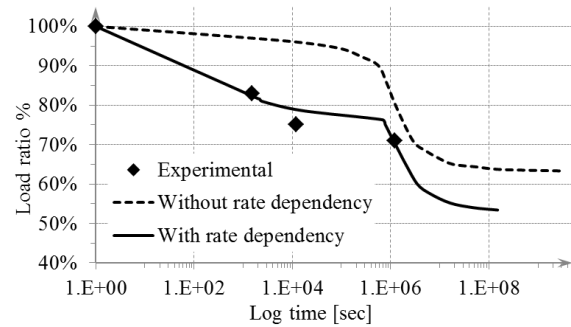


Figure 17: Effect of cracking strain rate.

### 8.4 Effect critical strain on time of failure

If the magnitude of the critical strain is changed to a lower value, e.g. 0.00014, the graph in Figure 18 may shift to the left as faster fracture is expected, but it would be also shifted up, as the ultimate capacity is decreased. Hence, the effect of critical strain on time of failure is insignificant.

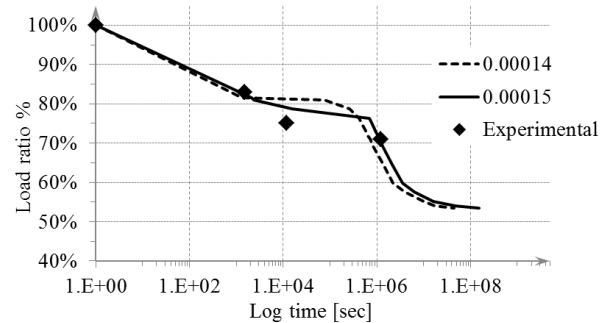


Figure 18: Effect of critical strain.

### 8.5 Effect of fracture energy mode I

The magnitude of the fracture energy in mode I cracking has an important influence on

the resistant stress in FPZ, accordingly the stress in front of the crack depends on  $I G_F$ ; a lower fracture energy leads to a higher stress at the crack tip and faster development of the crack.

### 8.6 Effect of fracture energy mode II on shear capacity

The effect of fracture energy in mode II cracking on short-term shear failure is presented in Figure 19. This result is obtained based on  $I G_F = II G_F$ . Obviously, when considering only fracture energy mode I, the fracture mode is not shear failure and the beam fails in flexural mode, while considering the mixed mode, the crack propagation is more likely to be the shear crack.

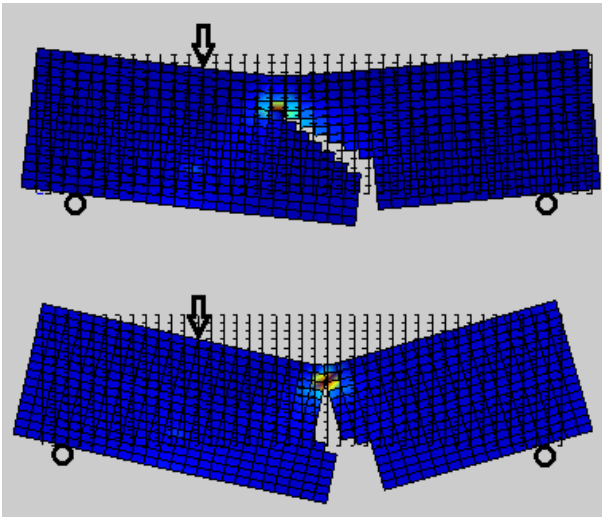


**Figure 19:** Crack propagation under deformed shape.  
Top: Fracture considering  $I G_F$  and  $II G_F$ .  
Bottom: Fracture considering  $I G_F$ .

## 9 CONCLUSION

To evaluate the shear capacity of concrete under sustained loading a finite element model is developed that takes into account the strain rate. This model has been validated against experimental results. For the crack development that may result in failure four different situations are distinguished as a function of the load ratio; see Figure 20.

- Load ratio higher than 75 to 80%: where the crack is initiated at time  $t_0=0$  and the cracking strain rate is taken into account, generating a fast propagation of the crack. As can be seen

in this figure, the total fracture occurs within 1000 seconds.

- Load ratio between 60 and 75%: where the crack does not occur at time  $t_0=0$ , but the potential cracks, denoted as micro-cracks, will in the long run be developed to a crack which becomes critical in a later stage and fracture occurs.

- Load ratio between 50 and 60%: where just a few micro cracks in the FPZ will develop in the long run, to finally make the strain exceeding its critical value

- Load ratio below 50%: where no crack is formed, and the stresses and strains are far from critical.

This paper presented the results of FE modeling together with a few experimental tests, which are in agreement with each other. However, for a better conclusion, further tests are required those are already undertaken. With the presented model, it is also possible to predict the shear crack process but in the absence of experimental data, the FE results are not given, although the results are similar to the flexural crack.

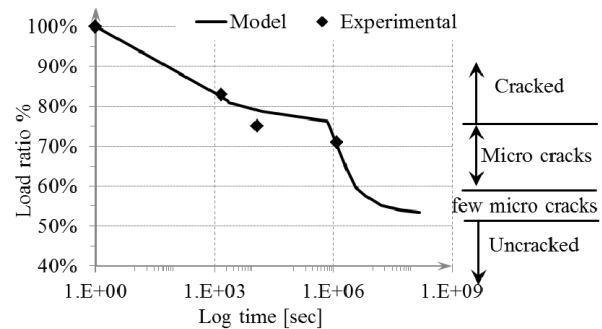


**Figure 20:** Estimated time for the fracture of the beam.

## REFERENCES

- [1] Barpi F., Chille, F., Imperato, L. and Valente, S., 1999, Creep induced cohesive crack propagation in mixed mode. In: Durban, D., Pearson, J.R.A. (Eds.), *Non-Linear Singularities in Deformation and Flow*. Kluwer Academic Publishers, The Netherlands, pp. 155–168.
- [2] Bažant, Z.P. and Wu, S. T., 1974. Rate-type creep law of aging concrete based on Maxwell chain, *Materials and Structures*

- (RILEM), 7 (No. 37), pp.45-60.
- [3] Van Zijl, G.P.A.G., de Borst R., and Rots J.G., 2001, The role of crack rate dependence in the long-term behaviour of cementitious materials, *Intl. J. Solids & Structures*, 38, pp.5063-5079.
- [4] Acker, P., Bažant, Z.P., Chern, J.C., Huet, C., and Wittmann, F.H., 1998, RILEM Recommendation on “Measurement of Time-Dependent Strains of Concrete”, (Subcomm. 4 RILEM Committee TC107-CSP). *Materials and Structures (RILEM, Paris)*, 31 (No. 212, Oct.), pp.507–512.
- [5] F.P. Zhou, A. Hillerborg, 1992, Time-dependent fracture of concrete: testing and modelling, In: Bazant, Z.P. (Ed.), *Fracture Mechanics Concrete Structures.*, The Netherlands, pp.906–911.
- [6] Di Luzio, G., 2009, Numerical Model for Time-Dependent Fracturing of Concrete, *Journal of Engineering Mechanics, ASCE*, Vol 135, No. 7, July 1, pp. 632-640.
- [7] Sarkhosh, R. 2012, Shear capacity of concrete beams under sustained loading. In Müller et al (eds), *Proc. of the 9<sup>th</sup> fib Inter. PhD Symp. in Civil Engrg.* July 2012, Karlsruhe, Germany; pp.29-34.
- [8] Chaimoon, K., Attard, M.M. and Tin-Loi F., 2008, Crack Propagation Due To Time-Dependent Creep in Quasi-Brittle Materials under Sustained Loading. *Comput. Methods Appl. Mech. Engrg.* 197, pp.1938-1952.
- [9] Bažant, Z.P. and Oh, B.H., 1983, Crack band theory for fracture of concrete. *RILEM*. 16(93), pp.155-177.
- [10] Bažant, Z.P., and Baweja, S., 2000, Creep and shrinkage prediction model for analysis and design of concrete structures: Model B3. In: ACI SP-194, A. Al-Manaseer, (ed.), *Adam Neville Symp.: Creep & Shrinkage-Struct. Design Effects*, Am. Concrete Institute, Farmington Hills, Michigan, pp.1–83.
- [11] Bažant, Z.P. and Chern, J.C., 1985, Strain-softening with creep and exponential algorithm. *J. of Engrg. Mechanics, ASCE* 111, pp.391–415.
- [12] Eurocode 2: Design of concrete structures (EN1992-1-1).
- [13] Bažant, Z.P. and Li, Y.N., 1997, Cohesive crack with rate-dependent opening and viscoelasticity: I. mathematical model and scaling. *Int. J. Fracture*, 86 (3), pp.247–265.
- [14] Collop, A.C, Scarpas, A., Kasbergen, C. and de Bondt, A., 2003, Development and FE implementation of a stress dependent Elasto-Visco-Plastic constitutive model with Damage for asphalt, *82<sup>nd</sup> TRB Annual meeting*, Washington DC.
- [15] Flugge, W, 1967, “Viscoelasticity”, Blaisdell Publishing Company, US.
- [16] Gálvez, J.C., Červenka, J., Cendón, D.A. and Saouma. V., 2002, A discrete crack approach to normal/shear cracking of concrete, *Cement and Conc. Research*, 3(2002), pp.1567-1585.
- [17] Hillerborg, A., Modéer, M. and Petersson P.E., 1976, Analysis of crack formation and crack growth in concrete by means of fracture mechanics and finite elements. *Cement Concrete Res.* 6: 773–782.
- [18] Petersson, P.E., 1981, Crack growth and development of fracture zones in plain concrete and similar materials. *Ph.D. Thesis, Lund Institute of Technology, Sweden.*
- [19] Bažant, Z.P., and Prat, P.C., 1988, Effect of temperature and humidity on fracture energy of concrete. *ACI Materials Jour.* 84, July 1988, pp.262–271.
- [20] CEB, "CEB-FIP Model code 1990", Buletin D'Information No 213/214, Lausanne, 1993.
- [21] Hilsdorf, H. K. and Brameshuber, W., 1991, Code-type formulation of fracture mechanics concepts for concrete. *Int. J. of Fracture*, Vol. 51, pp.61-72.
- [22] Xu S., 1999, Determination of parameters in the bilinear, Reinhardt’s nonlinear and exponentially nonlinear softening curves and their physical meanings. *Werkstoffe und Werkstoffprüfung im bauwesen*, Hamburg, Libri BOD, pp.410-424.